



Structural, Optical and Electrical Properties of Fe Doped SnO₂ Prepared by Spray Pyrolysis

C. Nassiri¹, A. Hadri¹, FZ. Chafi¹, A. El Hat¹, N. Hassanain¹,
M. Rouchdi¹, B. Fares¹, A. Mzerd^{1*}

¹LPM, Faculty of Sciences, Mohammed V University, B.P.1014, Rabat- Morocco

Received 08 Nov 2014,
Revised 25 Oct 2016,
Accepted 26 Oct 2016

Keywords

- ✓ Spray Pyrolysis,
- ✓ Fe-Doped SnO₂,
- ✓ thin film,
- ✓ Hall Effect.

mzerd@fsr.ac.ma (A.
Mzerd); Phone: +2126
61816454

Abstract

In this work, Iron-doped tin dioxide thin films were deposited on glass substrate heated at 350 °C by spray pyrolysis technique. Structural, optical and electrical properties of the films were investigated as a function of doping concentration ranging from 0 to 5 at % of Iron. X-ray diffraction analysis showed polycrystalline structure with clear characteristic peak of SnO₂ cassiterite phases in all films. Atomic Force Microscopy (AFM) reveals that film roughness is not affected by iron doping. From the optical measurements, it was observed that all films present a high transmittance in the visible range. Concerning the electrical measurements, it was found that the resistivity increased with increasing of Fe concentration

1. Introduction

Tin dioxide (SnO₂) thin film is well known as a wide band gap n-type semiconductor [1] with high simultaneous electrical conductivity and optical transparency in visible region of the spectrum [2]. It is considered as an interesting material for a wide array of applications like in light emitting and light triggered semiconductor devices, detectors, flat panel displays, solar cell arrays, heated windows, anti-static coatings, solid-state gas sensors, surge arresters (varistors) and oxidation catalysts [3–16]. Tin dioxide thin films have been prepared by several methods including reactive sputtering [17], thermal evaporation [18], chemical vapor deposition [19], sol gel [20], electrodeposition [21] and spray pyrolysis [22-24]. Among these techniques, spray pyrolysis is particularly attractive for metal oxide thin films elaboration. This technique is simple, cheap, and easily adaptable for large area deposition.

In this paper, we have focused our attention to investigate the effect of Fe doping on structural, optical and electrical properties of SnO₂ thin films using the inexpensive spray pyrolysis technique and a procedure which is very cost effective when compared to others.

2. Materials and methods

The samples of Sn_{1-x}Fe_xO₂ thin films were deposited on glass substrates by spray pyrolysis technique. The starting solution consisted of stannous chloride dehydrate (SnCl₂·2 H₂O) at a concentration of 0.035 M, dissolved in distilled water, where the water volume contained per liter of solution was fixed to 200 ml. The doping was achieved by the addition of iron chloride 4-hydrate (FeCl₂·4H₂O) to the solution, with a molar concentration of 0.053 M. The [Fe]/[Sn] atomic percent ratio explored in the solution were 0, 1, 3 and 5 at %. The substrate temperature was fixed to 350 °C and the solution was sprayed at a flow rate of 2.6 ml/min. The normalized distance between the spray nozzle and the substrate was 40 cm above the substrate. The X-ray

diffraction (XRD) D8-Advance X-ray powder diffractometer patterns of the samples are recorded using powder XRD (Cu K α radiation). Surface morphology of Fe doped SnO $_2$ thin films were performed by Atomic Force Microscopy (AFM, Dimension 3100). The optical transmittance of Fe-doped SnO $_2$ thin films was investigated by an UV/VIS spectrophotometer (Perkinelmer Lambda 900 UV/VIS/NIR). Electrical measurements were measured at room temperature using an ECOPIA Hall Effect Measurement System.

3. Results and discussion

3.1. Structural properties

The structural properties of undoped and Fe doped SnO $_2$ have been investigated by XRD. Typical X-ray diffraction spectra of the films are shown in Fig. 1. All diffractograms show only characteristic SnO $_2$ peaks and these peaks collaborate with ones from JCPDS 41-1445. The observed interplaner distance, d , values are presented in Table 1 and these values are compared with the standard ones from the JCPDS card no: 41-1445. The matching of the observed and standard ' d ' values confirms that the deposited films are of SnO $_2$ with cassiterite tetragonal structure. The (110) peak is the most intense peak which is observed for all samples. Although the second intense peak was (200), other peaks assigned as (101) and (211) were also observed. Similar results have been observed by the studies carried out by Babar et al. [25, 26].

The reflection intensities for each peak contains information being related to the preferential or random growth of polycrystalline thin films investigated by calculating the texture coefficient $TC_{(hkl)}$ for the planes using the following equation [27]:

$$TC_{(hkl)} = \frac{I_{hkl}/I_0}{(1/N) \sum I_{hkl}/I_0} \quad (1)$$

In this equation, $I_{(hkl)}$ is the measured relative intensity of a plane (hkl), $I_0(hkl)$ is the standard peak intensity of the plane (hkl) taken from JCPDS data no: 41-1445, N is the number of diffraction peaks. The calculated TC values are tabulated in Table 1.

The lattice constants ' a ' and ' c ', for tetragonal phase structure, are determined by the following relation [28]:

$$\frac{1}{d^2} = \left(\frac{h^2 + k^2}{a^2} \right) + \frac{l^2}{c^2} \quad (2)$$

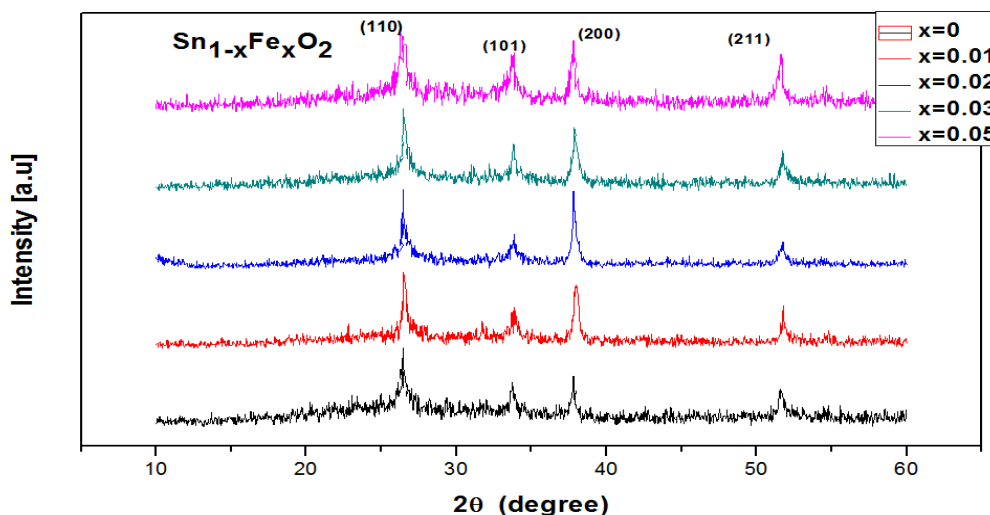


Figure 1: XRD patterns of Sn $_{1-x}$ Fe $_x$ O $_2$ thin films.

The observed lattice parameter ' a ' and ' c ' values are in concordance with standard value in JCPDS card no: 41-1445 ($a = b = 4.7382$ Å, $c = 3.1871$ Å), which indicates good crystalline nature of film. The average crystallites sizes (D) of the films are calculated from highly textured (110) and (200) peaks by using Scherrer formula [29]:

$$D = \frac{0.9\lambda}{\beta \cos \theta} \quad (3)$$

Where λ is the wavelength used (1.5405 Å), β is the full width at half of the peak maximum (FWHM) in radians and ' θ ' is Bragg's angle. The grain size values for (110) and (200) peaks are given in Table 1.

For (110) peak, the calculated D value for undoped film firstly increases from 13.46 nm to 20.35 nm with 1.0 at.% Fe doping and then decreases to 4.52 nm with 2.0 at.% Fe doping. The observed decrease in average crystallite size may be attributed to the enhancement of (200) orientation. The grain size increases again to 41.89 nm in doping levels higher than 3.0 at. %.

Table 1: The textured coefficient (TC), Lattice parameters (a) et (c) and mean grain size values of $\text{Sn}_{1-x}\text{Fe}_x\text{O}_2$ thin

	TC		D (nm)	Lattice parameters	
	110	200		a(Å°)	c(Å°)
Undoped SnO_2	1.56	0.51	13.46	4.76	3.22
SnO_2 :Fe (1%)	1.03	0.85	20.35	4.72	3.24
SnO_2 :Fe (2%)	1.03	1.02	04.52	4.76	3.22
SnO_2 :Fe (3%)	1.23	0.76	08.19	4.72	3.24
SnO_2 :Fe (5%)	1.23	0.61	41.89	4.76	3.22

3.2. Morphological properties

Figure 2 shows the AFM micrographs of SnO_2 doped with different iron concentrations. These micrographs illustrate that the substrates are entirely covered with grains of different sizes and reveal that the film deposited at lower dopant concentration lead to a more uniform and smoother surface values of root mean square roughness (RMS) and mean roughness (Ra) which are given in Table 2.

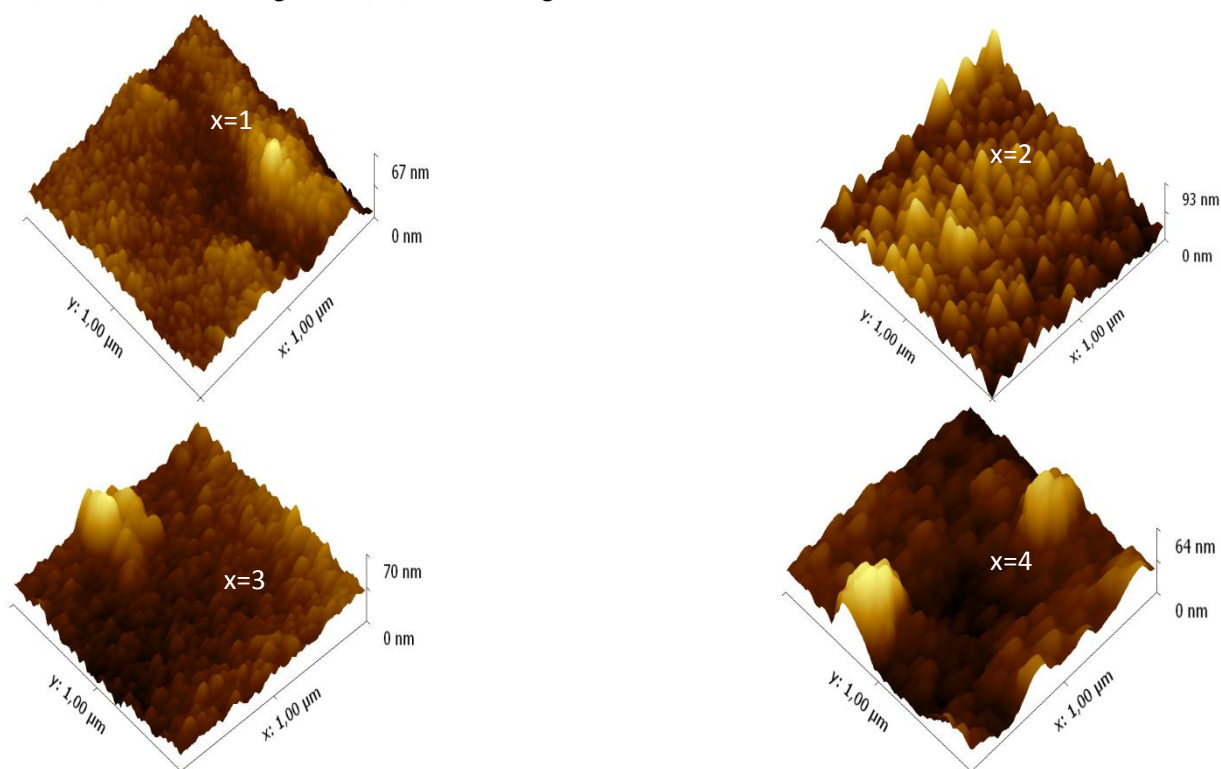


Figure 2: AFM images of $\text{Sn}_{1-x}\text{Fe}_x\text{O}_2$ thin films.

Table 2: Mean roughness and RMS values of Sn_{1-x}Fe_xO₂ thin films.

Surface Roughness (nm)		
X (at. %)	Mean Roughness R _a	RMS Roughness
0	7.3	9.7
1	7.8	9.8
3	10.2	13
5	17	20

The RMS roughness (see Table 2) increases with Fe doping. It can be also seen that the surface morphology changes depends on the amount of iron atoms in the films. This tendency may be caused by the agglomeration of crystallites due to the migration of Fe on the growing surface. As a result, larger grains are formed and RMS increased.

3.3. Optical properties

Optical properties of Fe doped SnO₂ thin films have been investigated by UV–VIS spectrometer at room temperature. Fig. 3 shows optical transmittance curves as a function of wavelength for the undoped and Fe doped SnO₂ thin films. From the transmittance curves, it is seen that the transmittance of undoped film is strongly affected by the Fe doping concentration. In fact, It is observed that transmittance shows decreasing tendency with Fe doping concentration. The observed decrease might be is attributed to modification of defects and disorder, which reduced the light passing through the film. The transmittance values were observed between 81% and 93% in [550-1100] nm, whatever the iron content.

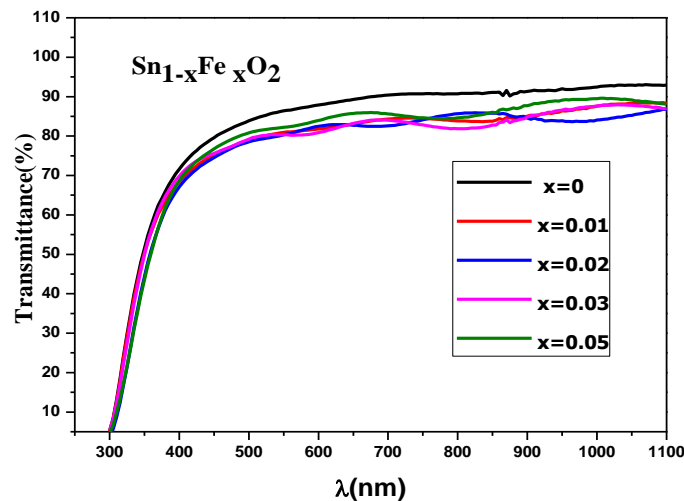


Figure 3: Optical Transmittance of Sn_{1-x}Fe_xO₂ thin films.

As a direct band gap semiconductor, the band gap energy (E_g) of Fe doped SnO₂ thin films is an important parameter. According the following formula E_g has a close relationship with absorption coefficient (α) and photon energy ($h\nu$) [30]:

$$\alpha h\nu = k(h\nu - E_g)^m \quad (4)$$

In Eqs (4), k is a constant related to the material E_g is the optical band gap, m is equal to $\frac{1}{2}$ for direct band gap and α is the absorption coefficient. Thus, E_g is found by extrapolating the straight line in the $(\alpha h\nu)^2$ versus $h\nu$

graph at $\alpha = 0$. The variations in E_g on changing the concentration of Fe are depicted in Fig. 4. The Thickness of deposited films was measured by using surface profilometer and was found approximately 330 nm (at 350 °C deposition temperature). Gap energy gradually decreases from 3.37 eV to 3.21 eV, which is related to the carrier density reduction and/or grain size variation [31]. In fact, variation of band might be explained in terms of electron concentration dependence of band gap shift in the Fe-doped SnO₂ films.

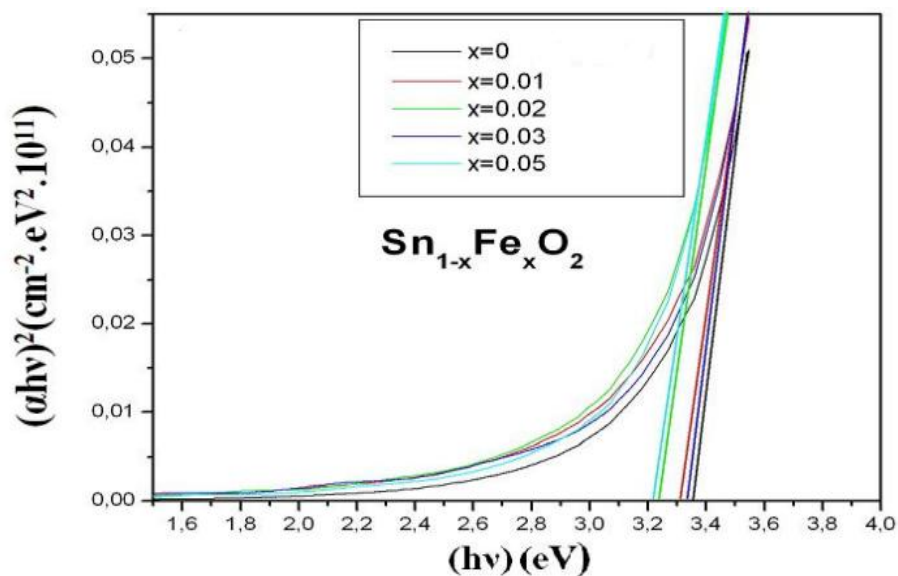


Figure 4: Plots of $(\alpha h\nu)^2$ versus $h\nu$ (photon energy) of Sn_{1-x}Fe_xO₂ thin films

3.4. Electrical properties

The room temperature electrical resistivity, mobility, and carrier concentration were measured by a standard Van-der-Pauw method and the average results are presented in Table 3. The electrical measurements show that the undoped and all iron-doped SnO₂ samples (pure SnO₂, 1%, 2%, 3%, 5% Fe) are n-type semiconductors. The values of the electrical parameters of SnO₂ are very different depending on Fe atomic content in the starting solution. Table 3 reveals that the resistivity increases with increasing Fe-doping which suggests that further doping leads to a substitution of the Sn⁴⁺ ions with Fe²⁺ ions. That has a direct effect on the carrier concentration density which decreases by doping. Tsay Chien-Yie and all also noticed the similar trend of resistivity and explained that the increase of resistivity is attributed to the compensation of electron for holes by increasing doping level [32]. On the other hand, this decrease in mobility values of 3% Fe doping might be attributed to the increase of ionized impurity. However, the Hall Effect experiment results confirm that the majority carriers levels are still electrons (n-type conduction).

Table 3: The electrical measurement results of of Sn_{1-x}Fe_xO₂ thin films.

Film+dopant	Resistivity (Ωcm)	Mobility(cm ² /V.s)	Carrier concentration (cm ⁻³)
Undoped SnO ₂	2.57×10^{-1}	4.42	-5.50×10^{18}
SnO ₂ :Fe (1%)	9.28	4.51	-1.49×10^{17}
SnO ₂ :Fe (2%)	7.65×10^1	5.44	-1.50×10^{16}
SnO ₂ :Fe (3%)	1.20×10^2	2.92	-1.78×10^{16}
SnO ₂ :Fe (5%)	1.07×10^2	9.44	-6.16×10^{15}

Conclusions

In this work, Iron-doped tin dioxide ($\text{SnO}_2\text{:Fe}$) are deposited by spray pyrolysis technique. The analysis of their structural, morphological optical and electrical properties is performed. The structural analysis performed indicates that the films have polycrystalline structure with clear characteristic peak of SnO_2 cassiterite phases. The $\text{SnO}_2\text{:Fe}$ thin films exhibit an average 85% transparency in the visible region, this value make this films suitable as an optical window for solar cells. The band gap slightly decreased with increasing Fe doping, which could be explained in terms of electron concentration dependence of band gap shift. The electrical behaviors show that the prepared iron-doped SnO_2 films are n-type semiconductors.

References

1. Nassiri C., Hadri A., Chafi F.Z., Loghmarti M., El Ammari L., Mzerd A., *Physical and Chemical News*, 72 (2014) 11.
2. Achour R., Atmane B., Chaker B., Boubaker B., Brahim G., *Superlattices and Microstructures*, 76 (2014) 105.
3. Das S., Jayaraman V., *Prog. Mater Sci.*, 66 (2014) 112–255.
4. Haider A.J., Shaker S.S., Mohammed A.H., *Energy Procedia*, 36 (2013) 776–787.
5. Ahmed Sk.F., Khan S., Ghosh P.K., Mitra M.K., Chattopadhyay K.K., *J. Sol–Gel Sci. Technol.*, 39 (2006) 241–247.
6. Wang Z., Liu L., *Mater. Lett.*, 63 (2009) 917.
7. Rani S., Roy S. C., Bhatnagar M. C., *Sensor. Actuat. B-Chem.*, 122 (2007) 204.
8. Korotcenkov G., *Sensor. Actuat. B-Chem.* 107 (2005) 209.
9. Garces F.A., Budini N., Koropecski R.R., Arce R.D., *Thin Solid Films*, 531 (2013) 172–178.
10. Shadia J. I., Riyad N.A., *Mater. Sci. Semicond. Process.* 12 (2009) 122–125.
11. Kotsikau D., Ivanovskaya M., Orlik D., Falasconi M., *Sensor. Actuat. B-Chem*, 101 (2004) 199.
12. Gu F., Wang S. F., Lu M. K., Qi Y. X., Zhou G. J., Xu D., Yuan D. R., *Opt Mater.*, 25 (2004) 59.
13. Hayakawa T., Nogami M., *Sci. Technol. Adv. Mater.*, 6 (2005) 66.
14. Timonah N.S., Chunhui Y., Liang S., *Mater. Sci. Semicond. Process.*, 13 (2010) 125-130.
15. Subramanian V., Gnanasekar K. I., Rambabu B., *Solid State Ionics*, 175 (2004) 181.
16. Taniguchi S., Yokozeki M., Ikeda M., Suzuki T.-k., *Jpn. J. Appl. Phys., Part 1* 50 (2011) 04DF11.
17. Xu B., Ren X.G., Gu G.R., Lan L.L. and Wu B.J., *Superlattices and Microstructures*, 89 (2016) 34.
18. Bhardwaj N., Pandey A. and Mohapatra S., *Journal of Alloys and Compounds*, 656 (2016) 647.
19. Lu Y.M., Jiang J., Becker M., Kramm B., Chen L., Polity A., He Y.B., Klar P.J. and Meyer B.K., *Vacuum*, 122 (2015) 347–352.
20. Köse H., Karaal Ş., Aydin A.O. and Akbulut H., *Mater. Sci. Semicond. Process.*, 38 (2015) 404.
21. Chen Z., Tian Y., Li S., Zheng H. and Zhang W., *Journal of Alloys and Compounds*, 515 (2012) 57.
22. Abdelkrim Al., Rahmane S., Abdelouahaba O., Abdelmalek N. and Brahim G., *Optik*, 127 (2016) 2653.
23. Chafi F.Z., Hadri A., C. Nassiri, B. Fares, L. Laanab, N. Hassanain, A. Mzerd, *J. Mater. Environ. Sci.*, 7(1) (2016) 170.
24. Riveros R., Romero E., and Gordillo G., *Brazilian Journal of Physics*, 36 (2006) 1042.
25. Babar A. R., Shinde S. S., Moholkar A. V., Bhosale C. H., Kim J. H., Rajpure K. Y., *J. Alloy. Compd.*, 505 (2010) 416.
26. Babar A. R., Shinde S. S., Moholkar A. V., Bhosale C. H., Kim J. H., Rajpure K. Y., *J. Alloy. Compd.*, 509 (2011) 3108.
27. Hadri A., Taibi M., loghmarti M., Nassiri C., Slimani Tlemçani T., Mzerd A., *Thin Solid Films*, 601 (2016) 7–12.
28. Chacko S., Philip N. S., Gophandran K. G, Koshy P., Vaidyan V. K., *Appl. Surf. Chem.*, 254 (2008) 2179.
29. Cullity B. D., Stock S. R., Elements of X-ray diffraction, 3rd ed, *Prentice Hall Publication*, (2001).
30. Michel C., Mejda A., Najoua K., *Optik*, 126 (2015) 708–714.
31. Serin T., Serin N., Karadeniz S., Sarı H., Tugluoglu N., Pakma O., *J. Non-Cryst. Solids*, 352 (2006) 209.
32. Tsay Chien-Yie, Liang Shan-Chien, *J. Alloys Comp.*, 622 (2015) 644.

(2017) ; <http://www.jmaterenvironsci.com/>